Contrib Mineral Petrol (2006) 151: 187–201
DOI 10.1007/s00410-005-0054-3

ORIGINAL PAPER

W. P. Meurer · M. E. S. Meurer

Using apatite to dispel the "trapped liquid" concept and to understand the loss of interstitial liquid by compaction in mafic cumulates: an example from the Stillwater Complex, Montana

Received: 10 May 2005 / Accepted: 30 November 2005 / Published online: 10 January 2006

Abstract The size, paragenetic setting, distribution, and composition of apatite grains in 16 thin sections from one sample of an olivine gabbro from the Stillwater Complex, Montana were documented to determine whether they grew from trapped interstitial liquid or in an open system. The grains show extreme variability in cross-sectional area, ranging from <150 to $>300{,}000$ μm^2. The apatite grains are not associated with quartz, Fe–Ti oxides, or evolved overgrowths on cumulus grains as expected for the crystallization of a trapped liquid, which suggests that they grew in an open system. The grains are very irregularly distributed, with a single cluster comprising almost 25% of the cumulative apatite cross-sectional area from all 16 slides. The spatial patterns of the apatite indicate that the interstitial liquid moved in tubular channels during the final stages of compaction. The trace-element composition of liquids calculated from apatite and silicate mineral compositions are similar, indicating that the apatite crystallized from liquids that were not dramatically enriched in incompatible elements. We conclude that the interstitial liquid never actually became trapped, that liquid was lost in an open system to essentially zero porosity, and that the model of cumulates as a combination of cumulus grains and trapped liquid should be discarded.

Editorial Responsibility: T. L. Grove

W. P. Meurer · M. E. S. Meurer
Department of Geology, Earth Science Centre,
Göteborgs University, Box 460, 405 30 Göteborg, Sweden

Present address: W. P. Meurer (✉)
Department of Geosciences, University of Houston, 312 Science and Research Building 1, Houston, TX 77204-5007, USA
E-mail: wpmeurer@mail.uh.edu
Tel.: +1-713-7430214
Fax: +1-713-7487906

Present address: M. E. S. Meurer
ExxonMobil Upstream Research Company, Houston, TX, USA

Introduction

In their classic text, Wager and Brown (1967) proposed that cumulates form from a mixture of cumulus grains and "trapped liquid" (p. 64). They defined trapped liquid as liquid that was in equilibrium with the cumulus grains at the time of their accumulation and is preserved as a mesostasis with a bulk composition equal to that of the equilibrium liquid composition. This simple model for fractional crystallization has important implications for understanding both the evolution of a fractionating liquid and the composition of the solid residue (cumulates). If fractionation proceeds in the manner proposed by Wager and Brown, then having more or less trapped liquid changes the volume of the remaining supernatant magma, but does not alter its compositional path as fractionation proceeds. The trapped liquid concept also greatly simplifies the treatment of bulk-chemical analyses of cumulates, since it implies that the proportion of trapped liquid can be calculated using any incompatible element. In practice, however, only the more strongly incompatible elements are used in these calculations (e.g., Henderson 1970; Cawthorn and Walsh 1988). The reason for this choice is made clear by Meurer and Boudreau (1998a) who show that if compaction takes place concurrent with crystallization, elements with higher bulk distribution coefficients yield higher estimates of the amount of trapped liquid.

Despite quantitative demonstrations of the shortcomings of the trapped liquid concept, its use persists (e.g., Bèdard 1994; Ross and Elthon 1997) primarily because it provides a convenient simplification of the fractionation processes. The trapped liquid concept allows numerical models of liquid evolution to neglect potential complications introduced by the return of variably fractionated liquids from the crystal pile (e.g., Langmuir 1989; O'Hara and Fry 1996a, b; Meurer and Boudreau 1998a). It also facilitates calculation of the composition of the cumulus portion of a cumulate, allowing bulk inversion techniques to be used to estimate

equilibrium liquid compositions (Bédard 1994, 2001) and providing a direct quantitative description of the instantaneous crystallizing assemblage. Even in studies that have recognized the limitations of the trapped liquid concept, its use persists. For example, Haskin and Salpas (1992) recognized that the thick anorthosites from the Stillwater Complex could not be adequately described by a mixture of cumulus plagioclase and trapped liquid. However, rather than investigating an open system model for the compositional variability of the cumulates, they used a three component system, including cumulus plagioclase, post-cumulus (but not evolved) pyroxene, and trapped liquid.

In this contribution we use the distribution and composition of apatite grains in an olivine gabbro from the Stillwater Complex, Montana, to describe the distribution of trapped liquid. If discrete pockets of liquid crystallized in this cumulate, then apatite (saturating in basaltic liquids after ≥90% fractionation) should identify those pockets. The expectation is that apatite should be associated with other late-stage minerals (e.g., Fe–Ti oxides, K-feldspar, and quartz) and evolved overgrowths on the cumulus minerals (e.g., more albitic rims on plagioclase). If, however, crystallization of interstitial liquid proceeds concurrent with compaction, then apatite might indicate how that liquid was distributed as the liquid fraction diminished to zero.

Methods and results

Sample petrography and mapping of apatite

We studied an olivine gabbro (M105) from ~10 m stratigraphically below the top of Olivine-bearing zone IV of the Middle Banded series of the Stillwater Complex, Montana (Lat. N45°26.847′, Long. W100°3.097′; Meurer and Boudreau 1996a). The sample is medium grained with most crystals between 2 and 6 mm in maximum dimension. Mineral proportions calculated by multiple linear regression of the mineral compositions against the bulk-rock composition give the following weight proportions of the major minerals: 7% olivine, 28% clinopyroxene, 12% orthopyroxene, and 52% plagioclase. Plagioclase and clinopyroxene occur as discrete, euhedral tabular grains, while olivine is subhedral with abundant inclusions of plagioclase. Orthopyroxene occurs interstitial to the minerals and locally as overgrowths on olivine. The plagioclase displays an igneous foliation defined principally by larger crystals (Fig. 1). No lineation is apparent in this sample (Meurer and Boudreau 1998b).

We mapped apatite grains with a maximum dimension of ≥5 μm using backscattered electron imaging combined with the X-ray counts from a wavelength dispersive spectrometer set to the P K_α position (see Meurer and Boudreau 1996b for details). We captured digital backscatter images of all grains and used them to determine cross-sectional areas of two sets of five thin sections cut perpendicular to the foliation plane, and two sets of three thin sections cut in the foliation plane (Fig. 2). The location of each grain was determined from the X–Y stage locations and used to construct maps from the multiple adjacent sections (Figs. 3, 4). Three paragenetic settings of apatite occur in this sample: (1) interstitial grains, (2) grains included in primary silicate minerals, and (3) grains in polyphase inclusions. These polyphase inclusions are interpreted to be the crystalline product of locally generated immiscible liquids (Loferski and Arculus 1993). Interstitial apatite grains are the largest in all sections. Grains that are included in other minerals or in polyphase inclusions are similar to each other in size and are relatively small. Meurer and Boudreau (1996b) provide a discussion of the different paragenetic settings of apatite grains.

The apatite grains are extremely heterogeneously distributed with some sections containing a few small grains and others containing many grains, including some that are relatively large. For example, section SV1-2 contains 16 grains and has a cluster of four grains that constitute ~23% of the total apatite by area in all 16 sections (Fig. 4). In contrast, SV2-5 contains only six small grains. The 10 largest grains out of a total of 160 in all 16 thin sections, account for ~42% of the total apatite by area. No linear arrays of apatite grains, as identified in oceanic gabbros, were observed (e.g., Meurer and Natland 2001).

Mineral major- and trace-element compositions

Apatite and plagioclase compositions were determined at Duke University using a Cameca Camebax electron microprobe. Standard analytical conditions were: 15 kV acceleration voltage, 15 nA cup current, 10 μm beam diameter, and 10–40 s counting times. For apatite analyses Cl, F, and P were counted first to minimize loss of these elements due to sample degradation by the beam. Natural mineral standards were used, including chlor- and fluorapatite checked against NaCl and CaF_2 for apatite analyses. OH was calculated by site difference (Cl + F + OH = 1 per formula unit). Care was taken to minimize problems related to diffusion of the halogens in apatite (Stormer et al. 1993) using strategies discussed elsewhere (Meurer and Boudreau 1996b; Meurer and Natland 2001; Willmore et al. 2000). Data were corrected using a Cameca Phi Rho Z (PAP) correction.

Trace-element compositions of apatite, plagioclase, clinopyroxene, and orthopyroxene were determined using a Cetac ASX-200 Nd-YAG UV laser for sampling and an HP-4500 quadrupole ICP-MS for analysis at Göteborgs Universitet, Sweden. Analyses were conducted in spot mode and beam diameters of 25–200 μm, minimum counting times of 30 s, and maximum times of 160 s. Sections were prepared with a thickness of ≥90 μm to maximize counting times and minimize the chances of drilling through the minerals. NIST 612 glass was used

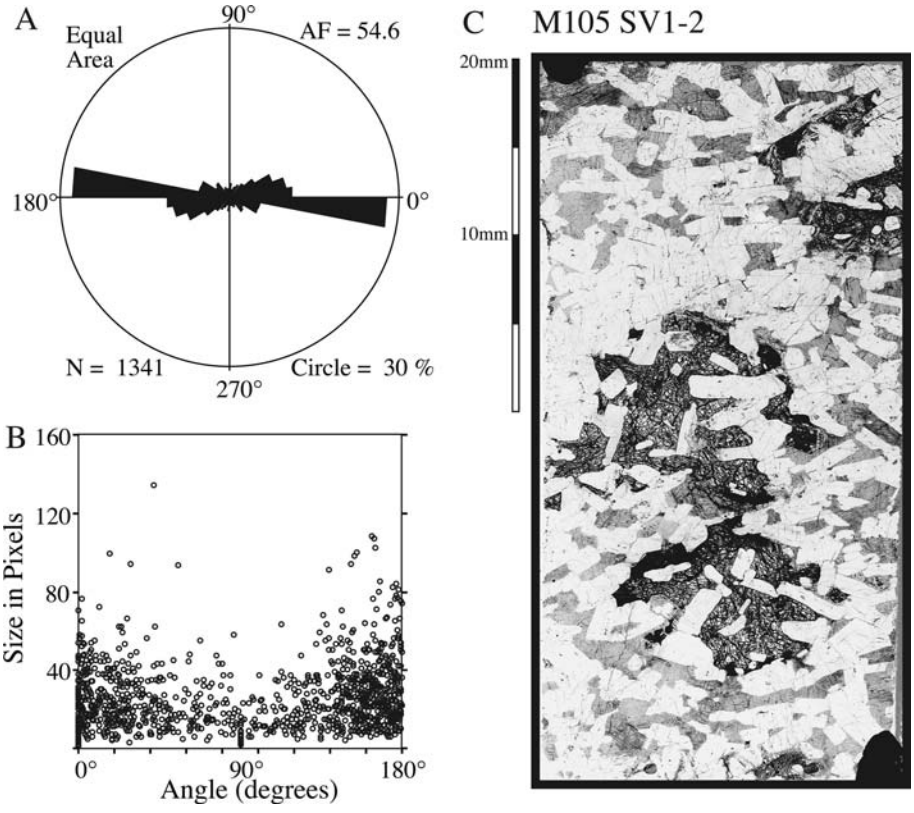

Fig. 1 **a** Rose diagram of plagioclase orientations. **b** Relationship between grain size (in pixels as measured by NIH image) and grain orientation as depicted in **a**. **c** Plain light image of slide SV1-2 (see Fig. 2). The dark fractured mineral in the *center* of the slide is olivine. Most of the *light gray* is clinopyroxene (with minor orthopyroxene) and plagioclase is colorless

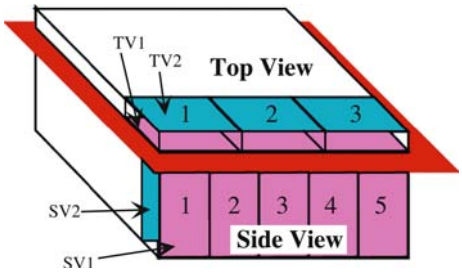

Fig. 2 Diagrammatic representation of sectioning of sample M105. The *dark plane* cutting the block represents the foliation plane, and the two sets of three and five adjacent sections show the locations of the 16 thin sections mapped. These are distinguished as *side view* and *top view* sets 1 and 2 with individual sections numbered sequentially as indicated. Short hand terminology for the side view, 1st set, 2nd section is SV1-2

as a standard for all analyses using the analytical approach described by Meurer and Claeson (2002). Estimated precision for a given element (x) is approximately based on concentration as follows (Meurer and Claeson 2002): $x \geq 10$ ppm ($\leq 5\%$), $0.25 \leq x \leq 10$ ppm ($\leq 10\%$), $0.05 \leq x \leq 0.25$ ppm ($\leq 20\%$), < 0.05 ppm ($\sim$20–50%).

Apatite major-element compositions conform to expectations based on earlier analyses of this sample and other nearby samples (Meurer and Boudreau 1996b). They show limited variability except in their OH-site occupancy as demonstrated by the apatite of a single section (SV2-1). In this sample, the mole fraction OH in the apatite (X_{Ap}^{OH}) varies between 0.4 and 0.5, but X_{Ap}^{Cl} ranges from 0.18 to 0.45, and X_{Ap}^{F} from 0.12 to 0.33 (Table 1). There is no systematic variation in the halogen content of the apatite with size (Fig. 5).

The trace-element compositions show considerably more variation than do the major elements (Table 2). For trace elements that are incompatible in cumulus minerals, concentrations in apatite are correlated with apatite grain size. For example, La concentrations vary by nearly a factor of 3 and are much higher in smaller grains (Fig. 6). All REE concentrations are highest in the smallest grains, and the chondrite-normalized REE patterns are sub-parallel for all grains (Fig. 7). Total variability is less for trace elements that are more compatible in the silicate minerals, and their concentrations are not as strongly correlated with size (Fig. 6). Sr concentrations vary by a factor of 2 and show a modest increase in concentration with the size of the grains. Mn concentrations also vary by a factor of 2 but show no correlation with size.

We analyzed plagioclase adjacent to interstitial apatite grains to determine if they preserve major-element zonation that might indicate crystallization from an increasingly evolved liquid (Table 3). However, none of the plagioclase showed significant zonation, and the modest zonation that is present shows an increase in An (molar Ca/molar Ca + Na) and a decrease in K_2O near apatite grain boundaries (Fig. 8). This holds true regardless of the size, habit, or local variations in the setting of the apatite grains. Similarly, no albitic rims have been documented on plagioclase grains elsewhere in this sample.

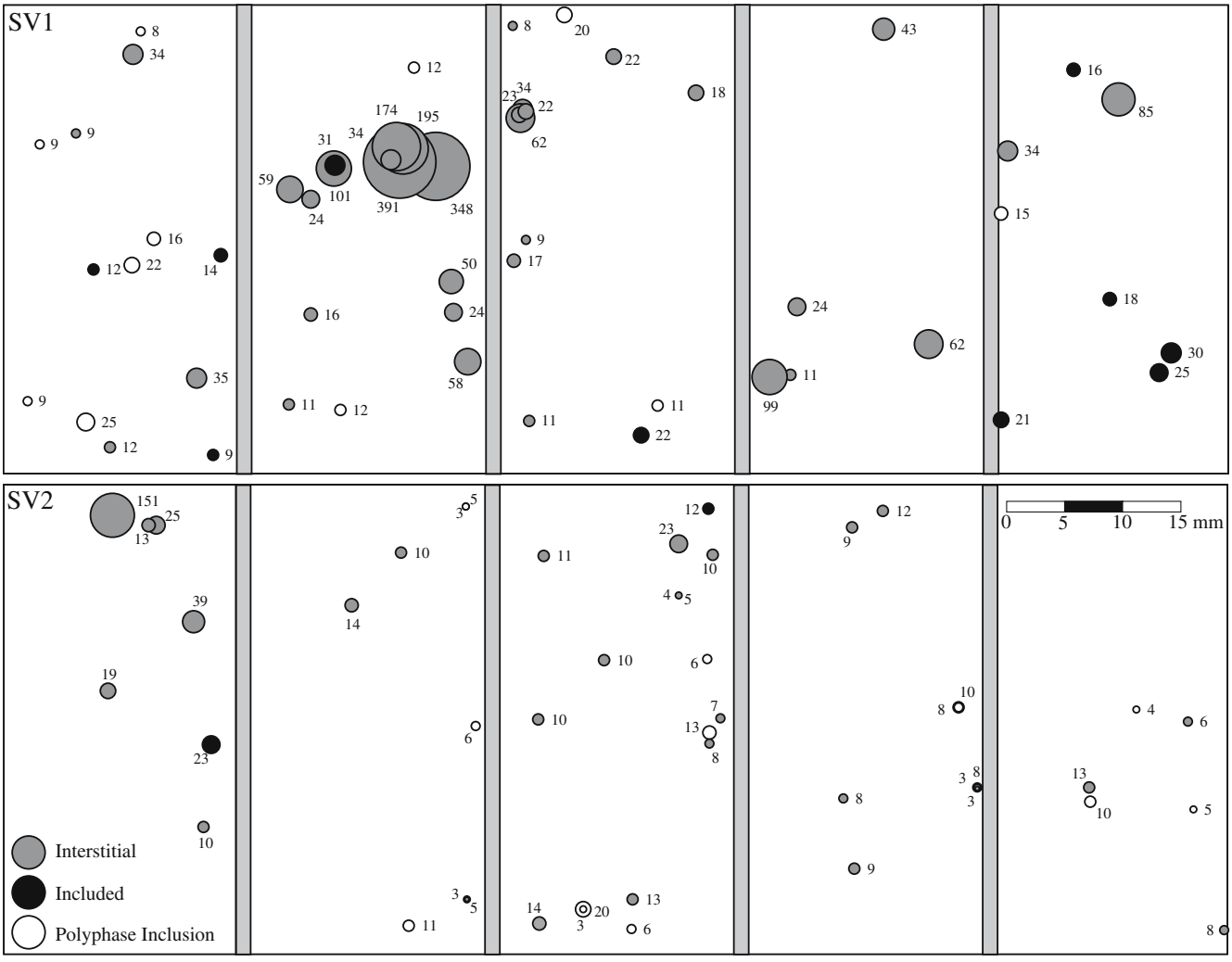

Fig. 3 The locations of apatite grains in two sets of five adjacent sections is depicted. The cut is perpendicular to the plane of the foliation and is referred to as the side view (*SV*) in the text. The area of each grain is reflected in the size of the *symbol*. The corresponding feret radius is also indicated. *Gray bars* indicate saw-cuts between sections where no apatite could be mapped

Trace-element compositions of plagioclase, clinopyroxene, and orthopyroxene were determined for comparison with the apatite compositions (Table 4). Analyses of cores and rims are similar, indicating minimal zonation for most elements (as resolved by the 100 and 200 μm laser analyses). Analyses from each mineral have subparallel chondrite-normalized REE patterns with shapes expected for equilibrium partitioning from the same liquid (Fig. 9). Significant variation of the heavy REE in plagioclase results from their concentrations approaching the detection limits. Orthopyroxene shows light REE concentration variations that are a mixture of analytical limitations and real compositional zonation.

Discussion

No evidence of trapped liquid

If the liquid interstitial to cumulus grains actually becomes trapped (i.e., the permeability of the system goes to zero), then the resulting crystallized assemblage must include all the minerals due to saturate with progressive fractionation. Quartz, magnetite, ilmenite, and titanite are commonly associated with apatite in anorthositic cumulates (Boudreau and McCallum 1989; Meurer and Boudreau 1996b). Therefore, it is logical to expect that apatite crystallized from trapped liquid in less-evolved cumulates, like M105, should be associated with other accessory minerals. Because this is not the case in any of the 16 sections examined, we conclude that the liquid the apatite crystallized from was not trapped. This conclusion is supported by the lack of evolved overgrowths on plagioclase grains adjacent to apatite grains. If the apatite crystallized from trapped liquid, then at some point the plagioclase that was crystallizing from that liquid must have also become relatively evolved. Yet what zoning is preserved in plagioclase is more anorthitic and less potassic immediately adjacent to the apatite (Fig. 9). We suggest that the apatite crystallized, not from a trapped liquid, but from

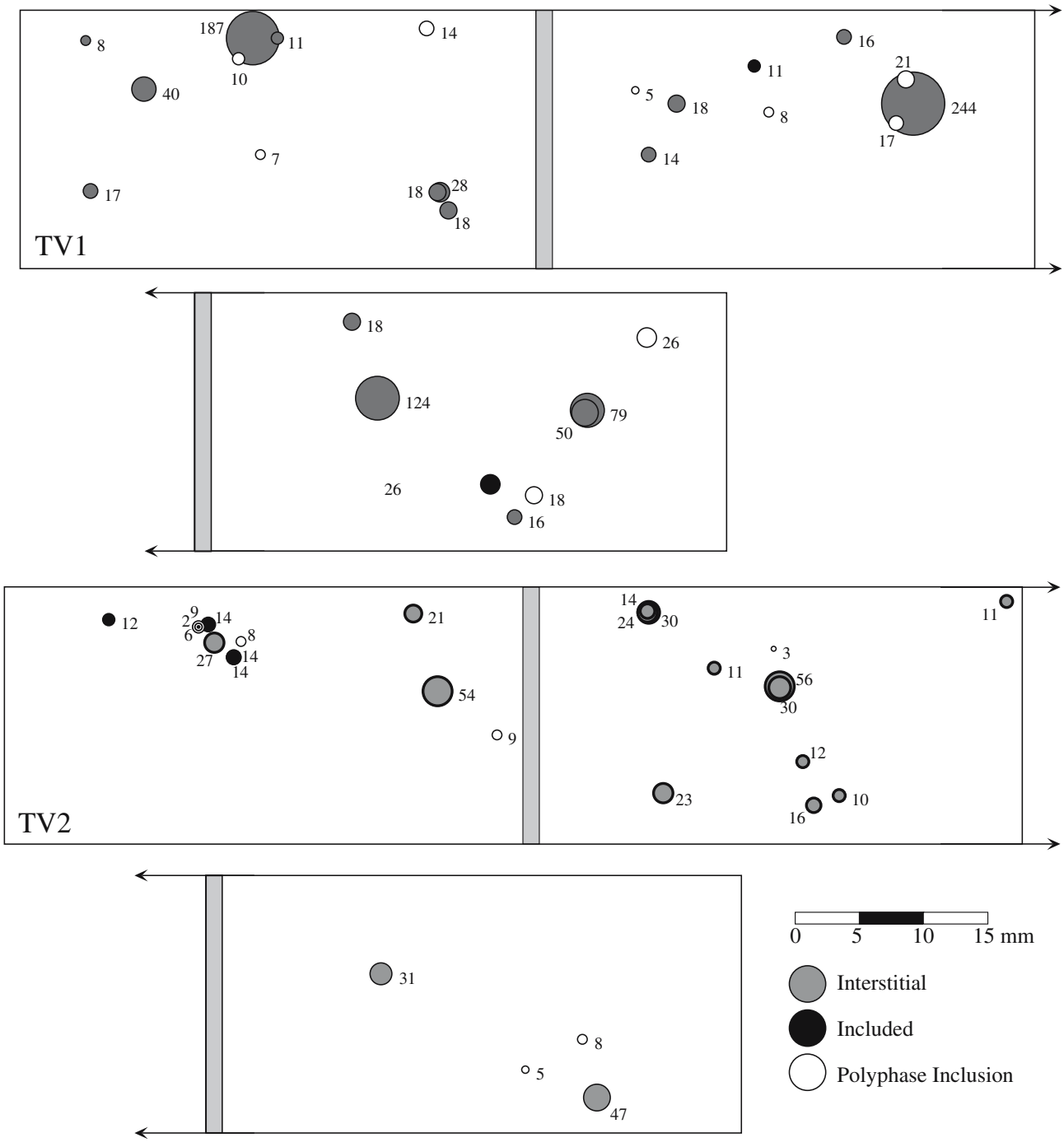

Fig. 4 The locations of apatite grains in two sets of three adjacent sections is depicted. The cut is in the plane of the foliation and is referred to as the top view (*TV*) in the text. The area of each grain is reflected in the size of the *symbol*. The corresponding feret radius is also indicated. *Gray bars* indicate saw-cuts between sections where no apatite could be mapped

an evolved liquid in the process of expulsion by compaction.

To support this interpretation we call attention to the large cluster of apatite grains in slide SV1-2 (Fig. 3). This cluster of four grains comprises ~25% of the total area of apatite in all 16 sections. If these grains crystallized from a trapped liquid with an initial P_2O_5 content of 0.2 wt%, then 30% of the area of the slide would have to have been trapped liquid in order to produce just these four grains. Crystallization of these four grains, without any associated quartz, Fe–Ti oxides, or evolved overgrowths on the cumulus grains, must have been from an evolved interstitial liquid that was expelled after apatite saturation. We can estimate the amount of interstitial liquid present upon apatite saturation for a basaltic liquid with an initial P_2O_5 content of 0.2 wt% that saturates in apatite at 2.0 wt% P_2O_5 with P behaving perfectly incompatible (thus ~92% fractional

Table 1 Microprobe analyses of apatite from thin-section SV2 (wt%)

Grain	Setting[a]	n[b]	X	Y	Size[c]	P_2O_5	CaO	SiO_2	FeO	Na_2O	Cl	F	OH	O ≡ F, Cl[d]	Total	X^{Cl}	X^{F}	X^{OH}
1	Inst	1	48245	9572	58	41.9	54.8	0.43	0.71	0.01	1.35	1.24	1.20	−0.83	100.8	0.19	0.33	0.47
5	Inst	2	47027	13767	24	41.7	54.3	0.34	0.32	0.00	3.06	0.49	1.06	−0.90	100.4	0.45	0.13	0.42
6	Include	1	46816	16384	50	41.5	54.7	0.31	0.41	0.03	3.00	0.46	1.11	−0.87	100. 7	0.43	0.12	0.44
8	Inst	28	45488	26215	348	41.0	54.0	0.66	0.52	0.01	2.49	0.66	1.13	−0.84	99.7	0.36	0.18	0.46
10	Poly	1	43625	34660	12	41.2	56.9	0.35	0.24	0.02	1.33	0.99	1.39	−0.72	101.7	0.18	0.26	0.56
11	Inst	25	42298	26575	391	41.2	55.0	0.28	0.12	0.01	1.92	0.72	1.33	−0.74	99.9	0.28	0.19	0.53
12	Inst	5	42629	27737	195	41.4	55.2	0.25	0.19	0.01	2.73	0.67	1.08	−0.90	100.6	0.39	0.18	0.43
13	Inst	10	42031	27909	174	40.8	54.3	0.45	0.31	0.01	1.68	0.71	1.39	−0.68	99.0	0.24	0.19	0.56
14	Inst	2	41635	26795	34	41.7	55.6	0.32	0.35	0.00	2.79	0.64	1.09	−0.90	101.7	0.40	0.17	0.43
15	Include	1	36806	26327	31	41.5	54.9	0.37	0.23	0.02	3.05	0.70	0.94	−0.98	100.8	0.44	0.19	0.37
16	Inst	6	36689	26029	101	42.5	55.4	0.12	0.06	0.00	1.99	0.78	1.31	−0.78	101.3	0.28	0.21	0.51
17	Poly	1	37278	5418	12	41.0	55.6	0.67	0.39	0.03	3.35	0.53	0.95	−0.98	101.6	0.48	0.14	0.38
18	Inst	1	34746	13554	16	42.2	55.5	0.85	0.70	0.00	2.82	0.44	1.23	−0.82	102.9	0.40	0.12	0.48
19	Include	1	34788	23389	24	40.3	52.4	0.42	0.69	0.04	1.61	0.78	1.32	−0.69	96.9	0.24	0.22	0.54
20	Inst	1	32844	5928	11	40.5	56.0	1.68	0.44	0.14	1.28	1.26	1.19	−0.82	101.6	0.18	0.33	0.49
21	Inst	2	32971	24260	59	41.4	56.5	0.13	0.05	0.01	1.84	0.84	1.31	−0.77	101.3	0.26	0.22	0.52

[a]Indicates the paragenetic setting of each grain (*inst* interstitial, *include* included in cumulus grain, *poly* in a polyphase inclusion)
[b]Indicates the number of analyses per grain
[c]Size represents the feret radius in microns
[d]Calculated weight percent of oxygen equivalent to the substituting F and Cl

crystallization is required to reach apatite saturation). For a sample that contains 40 vol% interstitial liquid that crystallizes in place, the fraction of liquid remaining in the rock would be 3.2 vol% at apatite saturation. If the initial liquid fraction is less then 40 vol%, then so would be the fraction of liquid remaining at apatite saturation. In M105 the very low concentrations of incompatible elements in the bulk rock indicate that as little as ~9 vol% or less of the sample may represent material crystallized from evolving interstitial liquid (Meurer and Boudreau 1998a). This means that as little as ~0.7 vol% of the sample was liquid when apatite began to crystallize. Given the absence of other late phases we conclude that the interstitial liquid was able to escape until the system reached essentially zero porosity.

An observation that deserves more attention is the absence of oxides and other accessory minerals in M105. Not only are these minerals not associated with apatite, but also, for the most part, they are absent entirely. This is curious because magnetite appears before apatite in the crystallization sequence of the Stillwater Complex and so is expected to saturate before apatite even if the interstitial liquid crystallizes as an open system. We suggest the reason that these accessory minerals are absent is the same as why the evolved overgrowths on plagioclase are absent—the interstitial liquid evolved along a different path from the main magma and became reactive with the solid assemblage (discussed in the following sections). Along this new path, apatite apparently saturates well before magnetite and quartz. It is likely that this is related to the buffering of the liquid by silicate minerals. For example, olivine would control the silica content, and both olivine and the pyroxenes would govern the Fe content of the evolving liquid.

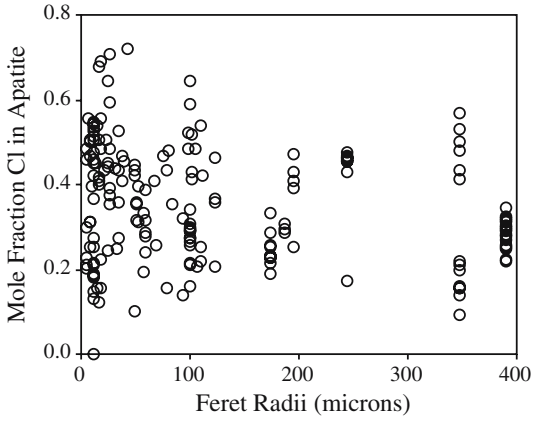

Fig. 5 X_{Ap}^{Cl} variation of individual microprobe analyses as a function of the feret radius of all apatite grains from the five SV1 sections and the three TV1 sections as described in Fig. 3

Evolution of the interstitial liquid

To understand how compaction could proceed with so little interstitial liquid remaining, it is necessary to consider its compositional evolution. The absence of either major- or trace-element zonation in the silicate minerals suggests minimal overgrowths and/or partial resorption of the solid assemblage by the liquid. Partial resorption (discussed in the following section) would explain the absence of evolved overgrowths on plagioclase (Fig. 8). The limited range in Sr and Mn in the apatite (Fig. 6) is also consistent with resorption of plagioclase, olivine, and/or clinopyroxene.

To examine the ability of the solid assemblage to buffer the incompatible element concentration of the liquid, we calculated REE concentrations for liquid in equilibrium with average pyroxene and plagioclase (Fig. 10). We used published liquid–mineral partition coefficients for clinopyroxene in these calculations

Table 2 Laser ICPMS analyses of apatites (ppm)

Section	Size	Sc	Ti	V	Mn	Co	Ni	Rb	Sr	Y	Zr	Nb	Cs	Ba	Pb	Th	U
SV1-2	391	4.2	98	80	281	4.0	2.0	2.1	146	185	25	0.32	0.07	26	6.6	90	8.7
SV1-2	348	7.5	113	76	270	3.8	2.9	1.5	145	170	21	0.26	0.11	23	6.7	86	7.3
SV1-2	195	3.0	138	85	430	2.0	19	ND	136	169	ND	0.13	0.20	106	9.2	93	9.6
SV1-2	174	15	94	94	323	3.1	5.7	0.24	137	178	15	0.36	bdl	16	8.2	122	13
SV1-2	101	22	106	79	309	4.6	20	5.6	110	281	25	0.81	0.03	25	17	253	20
SV1-2	59	15	135	47	396	2.2	12	2.5	123	337	34	1.6	bdl	40	18	234	18
SV1-4	62	2.4	102	75	246	8.2	21	1.4	116	471	18	bdl	0.10	39	26	341	38
SV1-5	30	65	622	121	365	13	37	0.77	84	516	8.9	bdl	bdl	28	15	207	23
SV1-5	85	3.2	97	83	199	2.0	1.2	0.87	139	303	6.6	bdl	bdl	18	12	145	18
TV1-2	244	16	829	143	435	13	38	1.5	169	223	20	0.18	0.13	13	24	255	30
TV1-3	124	2.8	147	74	271	1.3	9.4	0.38	148	374	8.0	0.16	0.02	19	18	200	30

Section	Size	La	Ce	Pr	Nd	Sm	Eu	Gd	Tb	Dy	Ho	Er	Tm	Yb	Lu
SV1-2	391	148	201	34	129	33	9.8	33	6.1	33	6.5	17	2.5	12	1.7
SV1-2	348	136	178	34	122	32	9.4	32	5.8	32	8.2	16	2.5	15	2.8
SV1-2	195	135	189	34	121	30	11	34	4.9	28	5.0	13	1.6	11	1.6
SV1-2	174	141	233	40	132	35	10	29	5.9	33	6.7	16	1.7	12	1.8
SV1-2	101	201	255	46	170	48	16	49	8.4	50	9.6	31	4.9	28	5.6
SV1-2	59	253	417	62	203	59	22	64	8.2	59	13	22	5.6	12	3.8
SV1-4	62	325	451	73	281	71	18	83	13	77	15	41	5.8	34	4.5
SV1-5	30	348	437	74	291	65	16	69	11	72	17	34	2.8	24	3.5
SV1-5	85	219	307	56	180	48	11	52	7.4	45	9.5	26	3.3	18	2.8
TV1-2	244	200	346	50	166	45	10	42	7.4	41	8.8	23	3.0	19	2.3
TV1-3	124	280	498	75	237	62	16	66	12	62	13	36	4.5	25	3.8

Size represents the feret radius in microns
ND Not determined, *bdl* below detection limit

(Table 5) and determined appropriate liquid–mineral partition coefficients for plagioclase and orthopyroxene using average mineral–mineral partition coefficients for five olivine gabbro(norites) from the Middle Banded series (unpublished data). The inversions of all three minerals give similar estimates of the equilibrium liquid composition, with the orthopyroxene inversion suggesting higher light REE concentrations. The latter reflects the larger range in LREE for orthopyroxene and its extremely small partition coefficients for these elements.

Inversion of apatite compositions for comparison with estimated liquid compositions from the cumulus mineral inversions is complicated by significant OH–F–Cl dependence of apatite REE partition coefficients (Fleet et al. 2000a, b). Changing proportions among OH, F, and Cl change the bond distances of the two discrete Ca sites in the apatite structure thereby changing the capacity for REE substitution. As the dominant anion in the OH-site changes from F (the smallest) to Cl (the largest), partition coefficients decrease creating the possibility that the REE could go from being strongly compatible in F-apatite to incompatible in Cl-apatite (Fleet et al. 2000a). The partitioning of the REE into apatite also depends upon other cation or vacancy substitutions that act to charge balance the +3 REE in the +2 Ca sites (e.g., Cherniak 2000). The relatively significant range in the OH-site occupancy observed in the apatite in M105 (Table 1), with F–Cl substitution being the most important variation, provides an additional complication to estimating partition coefficients. Rather than combining experimentally derived endmember partition coefficients, we have opted to use values determined from a Cl–F apatite in a glass-bearing mantle xenolith (Chazot et al. 1996) as discussed by Fleet and Pan (1997). Although the xenolith has a higher Mg# than the olivine gabbro considered here, the apatite grains in it have natural proportions of trace elements and so should provide partition coefficients appropriate for our purposes (Table 5).

Comparison of the liquid compositions derived from apatite with those based on the silicate minerals suggests that much of the apatite crystallized from liquids with REE concentrations near equilibrium with the silicate minerals (Fig. 10). In particular, the heavy REE concentrations estimated from the silicate minerals fall in the middle of the field defined by the apatite grains. The plagioclase and clinopyroxene light REE concentrations lie at the low end of those defined by apatite, while all silicate-based Eu concentrations fall below that estimated for the apatites. Because the partitioning of Eu is sensitive to the ratio Eu^{+2}:Eu^{+3}, the apparently anomalous behavior of Eu could result from using apatite partition coefficients appropriate for a different oxygen fugacity.

Apatite paragenesis

The systematic decrease in concentrations of those elements incompatible in the silicate assemblage with increasing apatite grain size suggests that the apatite grains grew from a liquid whose composition evolved during their crystallization. When the interstitial liquid

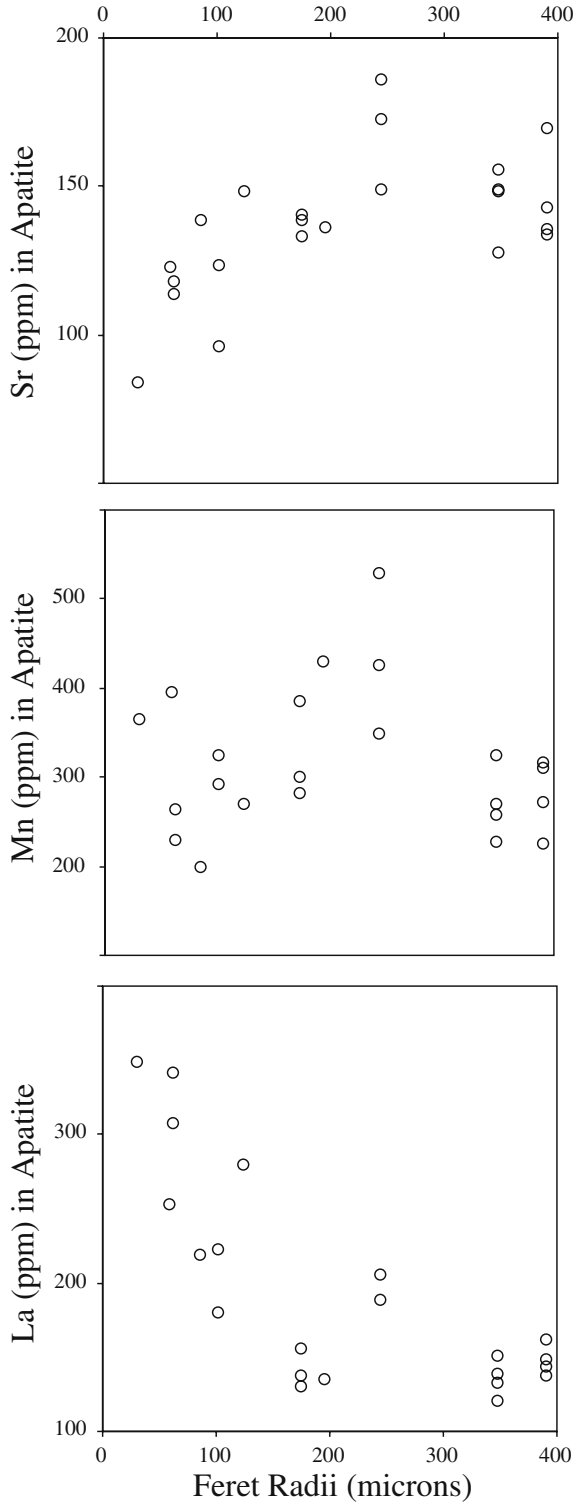

Fig. 6 Variation in Sr, Mn, and La concentrations by LA-ICP-MS as a function of the size of the apatite grains. Note that individual analyses are plotted so that multiple points at the same grain size represent multiple analyses of an individual grain. For Sr and Mn the within grain variability is large compared to the total variability. Estimated uncertainty for Sr, Mn, and La concentrations is smaller than symbol size

saturated in apatite, a burst of nucleation likely produced many small apatite grains. The addition of this apatite to the crystallizing assemblage caused a depletion of the REE. The first grains to grow under this scenario should have the highest REE concentrations. Continued growth then would be from a liquid with progressively lower REE concentrations. The addition of overgrowths with lower REE contents on the larger grains explains their lower total REEs.

If apatite growth started with the nucleation and growth of many small crystals, then the size of the individual grains can be taken as a measure of the amount of interstitial liquid locally available for continued growth. Both compaction of a crystal pile and crystallization of interstitial liquid act to decrease porosity and isolate apatite crystals. The widely distributed small apatite crystals indicate a relatively homogeneous distribution of interstitial liquid at initial apatite saturation, perhaps corresponding to an equilibrium liquid distribution (e.g., Faul 1997). However, the very clustered distribution of the largest apatite grains indicates that the liquid became increasingly localized as its volume decreased. We suggest that the evolving liquid became reactive with respect to the solid assemblage and so was no longer distributed in an equilibrium manner but became progressively channelized by reactive flow (e.g., Chadam et al. 1986; Kelemen et al. 1995; Meurer et al. 1997). Several lines of evidence suggest a reactive interstitial liquid. (1) The presence of a reactive interstitial liquid would explain the lack of evolved overgrowths on the plagioclase—plagioclase was actually being resorbed during apatite growth. (2) Resorption of plagioclase by a reactive liquid is also required to explain how the large euhedral apatite grains are accommodated between plagioclase grains as in SV1-2 (Fig. 8). The space occupied by these apatite grains is too large for it not to have been impinged upon by plagioclase during accumulation and compaction. (3) The resorption of silicate minerals would buffer compatible element concentrations, such as Sr and Mn, as is observed in the apatite compositions. (4) The absence of oxides associated with the apatite as expected from the crystallization sequence of the main magma reservoir of the Stillwater Complex also provides evidence that the evolution path of the interstitial liquid was different and therefore potentially reactive.

Using apatite to map liquid distributions

The crystallization of apatite from an increasingly reactive interstitial liquid provides a potential means of mapping the evolving liquid distribution as the porosity of a cumulate goes to zero. Mapping of apatite distributions in gabbros from the oceanic crust reveals that in many samples they define linear arrays that may be

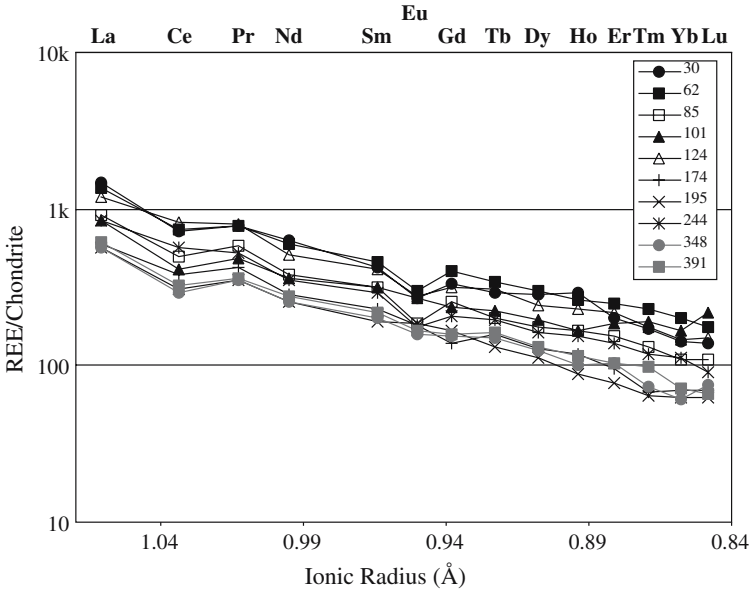

Fig. 7 Apatite REE concentrations normalized to chondritic concentrations (Sun and McDonough 1989) versus the ionic radius in angstroms of the REE (Shannon 1976). Note that the patterns are sub-parallel and that the smallest grains have the highest concentrations. The *legend* indicates the feret radius of the grain in microns for each pattern

interpreted as traces of planar flow pathways (Meurer and Natland 2001). Comparison of the three TV1 sections with the TV2 sections reveals that linear arrays identified in any given section do not appear in the corresponding section above/below (Fig. 5). Comparison of the five SV1 sections with the SV2 sections similarly reveals no matching linear arrays between corresponding sections (Fig. 4). Thus, the distribution of apatite grains provides no evidence for vertically oriented planar pathways. If the interstitial liquid migrated in vertically oriented fingers or tubes, then clusters or large apatite grains in the TV sections might occur centered above large concentrations of apatite grains in the SV sections. The largest concentration of apatite grains in a SV section is in SV1-2, in a position corresponding to near the end of the TV1(2)-1 section at the boundary with the TV1(2)-2 section. No concentration of apatite is found in this location in any of these four TV sections. The only remotely compelling correspondence of this sort is between the large apatite grain at the top of SV2-1 and the large grain in TV1-1 and cluster in TV2-1 (Figs. 4, 5).

The lack of any obvious paths defined by apatite grains in M105 could imply that arrays identified in the oceanic gabbros are merely coincidental. Alternatively, it could indicate that the slower cooling of the Stillwater cumulates allowed more competitive grain growth resulting in a greater spacing between apatite grains crystallized from the escaping interstitial liquid. The bulk of the smaller apatite crystals mapped in M105 likely correspond to grains that grew prior to significant focusing of flow of the interstitial liquid. Assuming that only the largest grains grew in well-established pathways for escape of interstitial liquid, then the initial spacing of these channels was at least 3–5 cm. The cluster of large grains found in SV1-2 likely represents the last active flow pathway in the sections studied. Because the fraction of interstitial liquid, and therefore the potential for additional growth of apatite is always decreasing, the size of this cluster is truly remarkable. The absence of a similar cluster in the other 15 sections suggests that the area studied is too small to constrain the spacing between the final channels that carried the most evolved liquid, beyond demonstrating that is must be at least 10 cm. The outcrop scale heterogeneity found in the thick anorthosites of the Stillwater Complex occurs at scales approaching a meter (Haskin and Salpas 1992) and likely provides an upper limit on channel spacing.

Implications for understanding interstitial liquid behavior

The most significant and straightforward implication of this work is that the model of cumulates as a mixture of cumulus grains and equilibrium "trapped liquid" should be discarded. Meurer and Boudreau (1998a, b), Ross and Elthon (1997); Boorman et al. (2004) have demonstrated that compaction occurs even after the interstitial liquid starts to solidify. Here we show that this process can go essentially to completion with practically all of the most evolved interstitial liquid removed. Numerical models of compaction of cumulates are based on porosity–permeability relationships that assume equilibrium behavior of interstitial liquid (e.g., Shirely 1986, 1987; Meurer and Boudreau 1996c). However, because evolved interstitial liquids can be reactive, a rigorous model for the end-stage crystallization and compaction in a crystal pile must include reactive transport. This approach is especially essential for intrusions that evolve more reactive interstitial liquids, such as those crystallizing from hydrous basaltic liquids (Meurer and Claeson 2002), or for those whose cooling history provide more time for compaction to occur. In these intrusions the cumulates should

Table 3 Microprobe analyses of plagioclase near apatites

	X	*Y*	SiO_2	Al_2O_3	FeO	CaO	Na_2O	K_2O	Sum	An
Ap-21 line#1	33272	24240	49.7	32.4	0.44	15.8	2.39	0.10	100.8	78.5
Ap-21 line#1	33261	24240	47.8	32.4	0.28	16.6	2.18	0.09	99.3	80.8
Ap-21 line#1	33250	24240	48.9	32.1	1.98	15.4	2.39	0.07	100.8	78.1
Ap-21 line#1	33239	24240	48.7	32.0	2.25	14.8	2.35	0.07	100.1	77.7
Ap-21 line#1	33228	24240	48.2	32.2	0.43	16.2	2.37	0.08	99.5	79.0
Ap-21 line#1	33217	24240	48.2	32.0	0.42	16.0	2.40	0.10	99.3	78.7
Ap-21 line#1	33206	24240	48.4	32.4	0.50	16.2	2.51	0.09	100.2	78.1
Ap-21 line#1	33195	24240	48.6	32.6	0.29	16.3	2.46	0.09	100.3	78.5
Ap-21 line#1	33183	24240	48.0	31.5	0.42	18.2	2.58	0.08	100.8	79.6
Ap-21 line#1	33172	24240	49.4	32.0	0.40	15.9	2.68	0.08	100.5	76.7
Ap-21 line#1	33161	24240	49.3	31.9	0.31	16.1	2.67	0.08	100.4	77.0
Ap-21 line#1	33150	24240	48.9	31.7	0.42	16.1	2.60	0.12	99.9	77.4
Ap-21 line#1	33139	24240	49.1	31.8	0.51	16.0	2.60	0.13	100.1	77.3
Ap-21 line#1	33128	24240	46.9	31.4	2.69	16.2	2.56	0.08	99.9	77.8
Ap-21 line#1	33117	24240	48.4	31.3	2.28	15.2	2.47	0.11	99.7	77.3
Ap-21 line#1	33106	24240	49.3	32.2	0.38	16.1	2.61	0.12	100.7	77.3
Ap-5 line#1	47349	13733	47.1	33.5	0.41	17.8	1.80	0.05	100.7	84.5
Ap-5 line#1	47347	13743	48.3	32.5	0.29	16.6	2.25	0.09	100.1	80.3
Ap-5 line#1	47345	13754	48.7	32.5	0.46	16.3	2.42	0.10	100.5	78.8
Ap-5 line#1	47343	13764	49.0	32.4	0.50	16.0	2.43	0.09	100.4	78.4
Ap-5 line#1	47342	13775	48.4	32.0	0.44	16.0	2.51	0.10	99.5	77.9
Ap-5 line#1	47340	13785	48.5	31.4	2.17	14.6	2.41	0.11	99.2	77.0
Ap-5 line#1	47338	13796	48.4	32.1	0.40	16.0	2.39	0.11	99.4	78.7
Ap-5 line#1	47336	13806	48.2	32.1	0.43	16.0	2.36	0.10	99.2	78.9
Ap-5 line#1	47334	13816	49.0	32.9	0.67	15.6	2.05	0.09	100.3	80.8
Ap-5 line#1	47332	13827	48.4	32.2	0.55	16.3	2.47	0.10	100.0	78.5
Ap-5 line#1	47330	13837	48.3	32.3	0.34	16.1	2.46	0.11	99.5	78.3
Ap-5 line#1	47329	13848	48.3	32.0	0.49	16.0	2.35	0.09	99.2	79.0
Ap-5 line#1	47327	13858	48.5	32.2	0.51	16.0	2.34	0.11	99.6	79.1
Ap-5 line#1	47325	13869	49.4	32.1	0.41	16.2	2.34	0.09	100.5	79.3
Ap-5 line#1	47323	13879	48.7	32.1	0.49	16.0	2.20	0.09	99.6	80.1
Ap-8 line#1	45673	26208	46.9	33.2	0.31	16.3	1.85	0.05	98.6	82.9
Ap-8 line#1	45673	26219	47.8	33.1	0.29	15.8	2.06	0.09	99.0	80.9
Ap-8 line#1	45673	26229	48.1	32.8	0.37	15.3	2.12	0.08	98.9	80.0
Ap-8 line#1	45673	26240	49.1	33.0	0.19	15.6	2.24	0.07	100.2	79.4
Ap-8 line#1	45673	26250	48.4	32.7	0.30	15.6	2.26	0.08	99.3	79.3
Ap-8 line#1	45673	26261	48.4	32.4	0.35	15.4	2.29	0.10	99.0	78.9
Ap-8 line#1	45673	26271	48.8	32.2	0.26	15.4	2.42	0.11	99.2	77.9
Ap-8 line#1	45673	26282	49.1	32.4	0.35	15.5	2.48	0.12	99.9	77.5
Ap-8 line#1	45673	26292	49.1	32.6	0.37	15.4	2.41	0.12	100.0	77.9
Ap-8 line#1	45673	26303	49.1	32.8	0.30	15.6	2.37	0.10	100.3	78.5
Ap-8 line#1	45673	26313	49.1	32.3	0.43	15.2	2.44	0.11	99.5	77.5
Ap-8 line#1	45673	26324	49.2	32.9	0.44	15.8	2.43	0.12	100.9	78.2
Ap-8 line#1	45673	26334	48.3	32.5	0.41	15.4	2.38	0.11	99.1	78.1
Ap-8 line#1	45673	26345	48.4	32.6	0.48	15.7	2.39	0.10	99.8	78.4
Ap-8 line#1	45673	26355	48.5	33.0	0.55	15.8	2.38	0.10	100.3	78.6
Ap-8 line#1	45673	26366	48.3	33.3	0.44	15.9	2.36	0.11	100.4	78.8
Ap-8 line#1	45673	26376	48.6	33.0	0.52	15.9	2.25	0.09	100.5	79.6
Ap-8 line#1	45673	26387	48.4	32.0	0.39	15.6	2.29	0.11	98.7	79.0
Ap-8 line#3	45657	26137	47.7	33.5	0.37	17.4	1.55	0.05	100.6	86.2
Ap-8 line#3	45653	26131	47.2	33.6	0.44	17.4	1.52	0.05	100.3	86.4
Ap-8 line#3	45649	26125	47.2	33.0	0.59	17.3	1.56	0.06	99.8	86.0
Ap-8 line#3	45645	26118	47.2	33.3	0.44	17.3	1.58	0.04	99.9	85.8
Ap-8 line#3	45641	26112	47.2	33.8	0.48	17.4	1.61	0.05	100.5	85.7
Ap-8 line#3	45638	26106	47.2	33.3	0.57	17.1	1.61	0.05	99.9	85.5
Ap-8 line#3	45634	26100	47.1	33.2	0.60	17.3	1.55	0.05	99.8	86.0
Ap-8 line#3	45630	26093	46.7	33.1	0.53	17.1	1.51	0.05	99.1	86.2
Ap-8 line#3	45626	26087	47.1	33.9	0.58	17.6	1.52	0.03	100.7	86.5
Ap-8 line#3	45622	26081	46.6	33.0	0.46	17.5	1.64	0.03	99.2	85.5

The first analysis in each traverse is adjacent to an apatite grain. See Fig. 8 for locations of traverses
X and *Y* provide stage locations for analyses and correspond to distances in microns

be described as a mixture of cumulus grains and a crystallized-liquid fraction to represent material that crystallizes during compaction. The crystallized-liquid fraction does not depend upon on a point at which the liquid becomes "trapped" in the sense that the permeability goes to zero, rather it is governed by the relative rates of heat loss and compaction (c.f., Meurer and Boudreau 1998a, b).

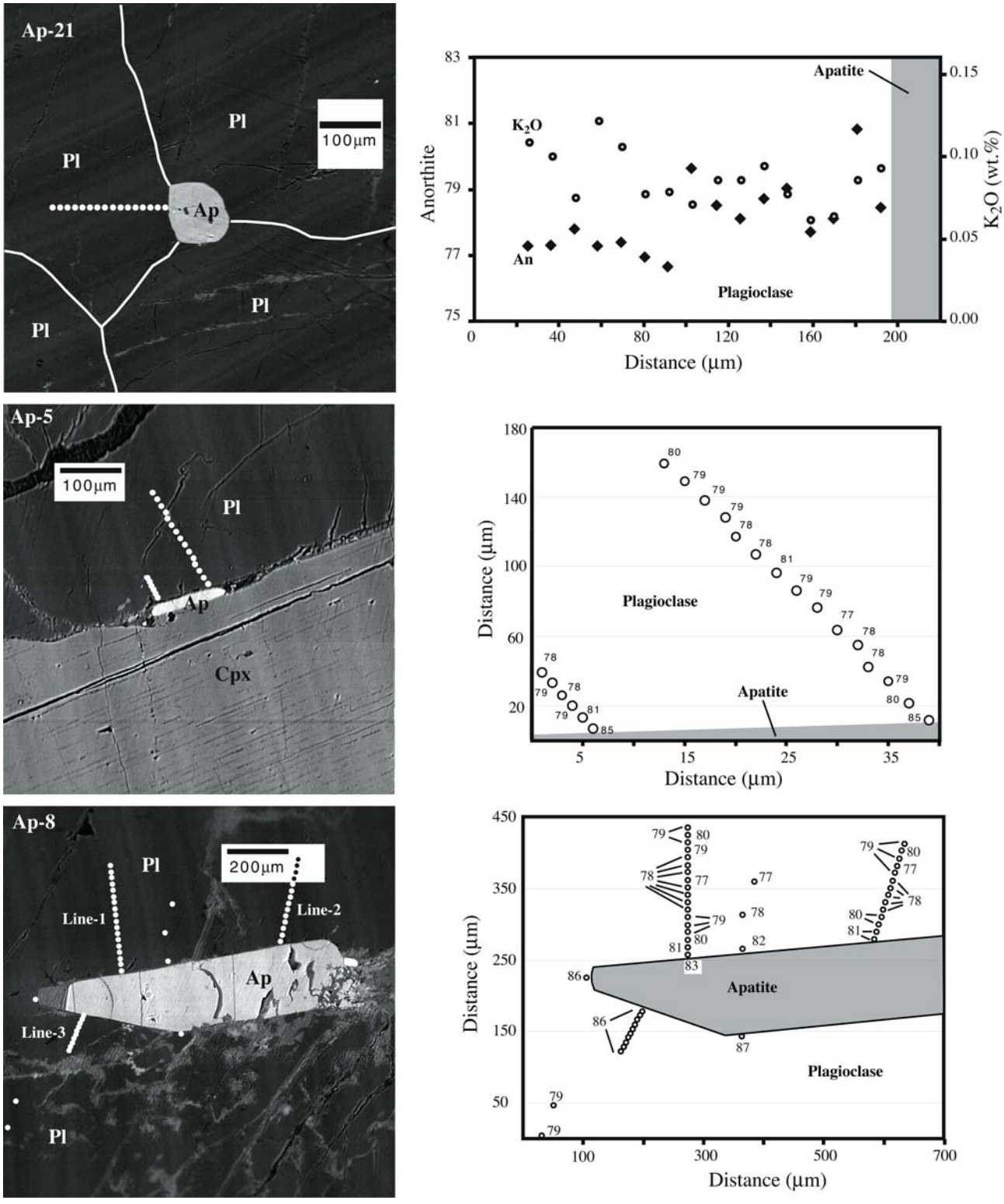

Fig. 8 Backscattered electron images and corresponding compositional maps of plagioclase adjacent to apatite grains. The *white dots* on the backscattered images indicate analyses points plotted on the *right*. Mineral abbreviations on images are: *Ap* apatite, *Pl* plagioclase, and *Cpx* clinopyroxene. The number of each apatite grain and compositional traverses are indicated for reference in Table 3. The values in the *lower two plots* at *right* indicate the An content of the plagioclase at that location

The process of reactive flow envisioned here has important implications for the evolution of the interstitial liquid that may be returned to the main magma reservoir during fractional crystallization. Two effects need to be considered: (1) the potential crystallization of accessory minerals, such as apatite, during loss of the

Table 4 Laser ICPMS analyses of silicate minerals (ppm)

Sc	Ti	V	Co	Ni	Rb	Sr	Y	Zr	Nb	Ba	La	Ce	Nd	Sm	Eu	Gd	Dy	Er	Yb	Lu	Pb	Th	U
Plagioclase																							
0.9	214	5.5	0.3	0.5	0.76	179	0.24	0.03	0.01	40	0.80	1.5	0.59	0.11	0.28	0.081	0.056	0.028	0.023	0.007	0.45	0.001	0.004
0.8	262	4.4	0.7	0.9	0.52	195	0.18	0.02	0.01	46	1.19	2.0	0.66	0.09	0.31	0.058	0.051	0.014	0.010	0.002	0.57	bdl	bdl
0.9	210	4.8	1.2	6.0	0.44	145	0.17	0.03	0.02	33	0.60	1.2	0.39	0.08	0.21	0.059	0.035	0.017	0.014	0.003	0.40	0.013	0.002
0.8	201	4.9	2.1	11	0.87	157	0.17	0.02	0.02	35	0.71	1.3	0.46	0.08	0.23	0.058	0.027	0.014	0.006	0.001	0.38	0.001	bdl
0.9	210	6.4	0.6	9.6	0.53	172	0.18	0.03	0.01	40	0.60	1.3	0.50	0.09	0.29	0.058	0.044	0.008	0.008	0.001	0.46	bdl	bdl
0.8	242	4.4	1.6	14	3.2	172	0.18	0.01	0.00	55	0.95	1.7	0.58	0.07	0.28	0.045	0.043	0.029	0.015	0.005	0.45	0.003	bdl
0.6	221	4.2	6.0	2.7	0.65	185	0.21	0.02	0.02	41	1.13	1.9	0.71	0.11	0.32	0.087	0.060	0.021	0.022	0.007	0.56	0.008	0.006
0.6	241	3.4	18	1.9	0.98	156	0.17	0.02	0.00	38	1.23	1.9	0.55	0.10	0.24	0.054	0.020	0.015	bdl	bdl	0.64	bdl	bdl
Orthopyroxene																							
48	2,171	205	87	301	0.02	0.23	4.04	4.1	0.03	0.28	0.03	0.06	0.10	0.04	0.02	0.18	0.47	0.55	0.89	0.18	0.03	0.04	bdl
49	2,210	204	83	294	0.10	0.45	4.24	4.2	0.05	0.87	0.06	0.09	0.11	0.08	0.02	0.19	0.49	0.56	0.86	0.17	0.04	0.13	0.02
47	2,111	208	78	287	0.23	0.71	4.08	4.6	0.07	1.4	0.09	0.15	0.15	0.09	0.02	0.16	0.46	0.53	0.78	0.16	0.03	0.12	0.01
46	2,095	209	79	287	0.67	2.3	3.68	3.7	0.05	2.7	0.15	0.27	0.22	0.11	0.03	0.24	0.44	0.49	0.80	0.15	0.05	0.07	0.02
44	2,266	213	85	312	0.73	1.8	3.68	3.6	0.08	3.3	0.17	0.23	0.24	0.12	0.03	0.29	0.41	0.41	0.87	0.18	0.04	0.10	0.04
48	2,368	224	87	302	0.12	0.78	3.73	3.6	0.04	1.2	0.09	0.17	0.15	0.08	0.02	0.16	0.38	0.46	0.81	0.16	0.34	0.09	0.03
45	2,496	222	89	314	0.26	0.75	3.60	3.7	0.04	1.9	0.05	0.11	0.14	0.09	0.02	0.17	0.37	0.42	0.80	0.15	0.06	0.11	0.02
Clinopyroxene																							
102	3,441	491	34	149	0.12	6.1	20.9	30	0.41	1.3	1.14	3.8	4.3	1.6	0.42	2.4	3.4	2.2	2.1	0.32	0.07	0.28	0.06
101	3,533	474	31	131	0.08	5.5	20.3	31	0.38	0.50	1.07	3.7	4.4	1.7	0.44	2.4	3.3	2.1	2.0	0.32	0.09	0.31	0.05
93	2,591	417	33	161	0.18	7.0	17.2	16	0.51	2.7	1.05	3.3	3.6	1.4	0.37	2.0	2.7	1.8	1.8	0.28	0.07	0.41	0.08
103	3,635	459	29	133	0.12	5.6	21.2	34	0.49	1.2	1.15	3.5	4.5	1.7	0.41	2.5	3.4	2.1	2.0	0.31	0.07	0.48	0.06
103	2,155	397	37	152	0.05	6.1	18.3	15	0.49	0.67	1.11	3.2	3.6	1.4	0.36	2.0	2.7	1.8	1.8	0.28	0.06	0.45	0.07
97	2,646	452	35	162	0.14	6.8	19.1	22	0.52	2.1	1.17	3.6	4.0	1.5	0.39	2.2	3.0	2.0	2.0	0.29	0.08	0.47	0.08
111	3,017	515	46	211	0.31	6.2	22.2	28	0.48	1.2	1.21	3.7	4.3	1.7	0.44	2.5	3.4	2.3	2.3	0.35	0.10	0.44	0.04
104	2,417	455	36	157	0.16	7.2	16.5	13	0.47	2.1	1.00	2.7	3.1	1.2	0.33	1.9	2.5	1.7	1.7	0.26	0.06	0.42	0.08
105	2,239	450	40	173	0.14	6.6	16.2	12	0.45	2.2	0.94	2.6	2.9	1.1	0.32	1.7	2.5	1.6	1.6	0.26	0.07	0.41	0.06
100	3,187	490	31	139	0.12	5.7	19.1	25	0.50	1.0	1.10	3.4	4.0	1.5	0.41	2.3	3.1	2.0	1.9	0.29	0.07	0.40	0.07

bdl Below detection limit

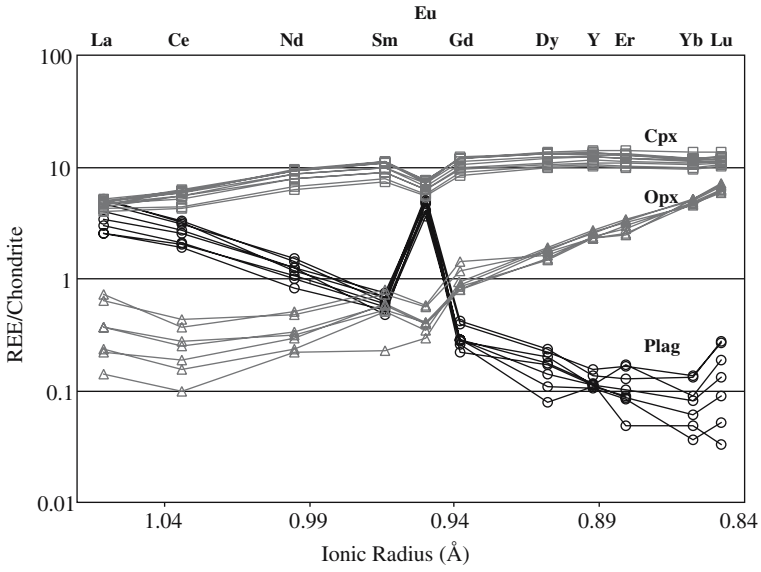

Fig. 9 REE concentrations normalized to chondritic concentrations (Sun and McDonough 1989) for plagioclase, clinopyroxene, and orthopyroxene plotted against the ionic radius in angstroms of the REE (Shannon 1976)

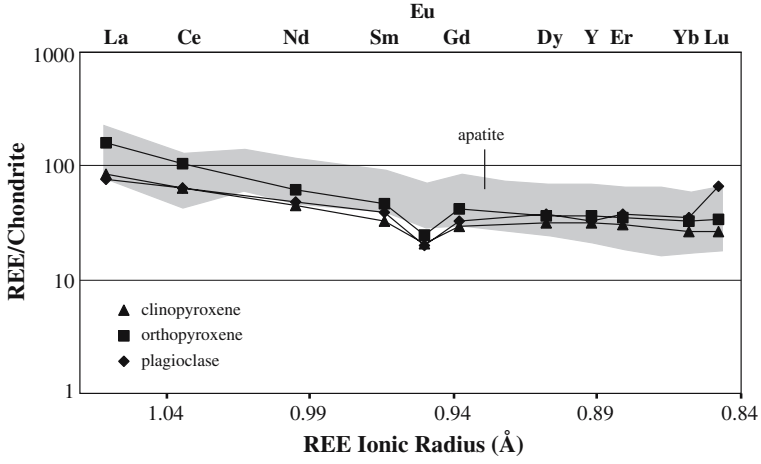

Fig. 10 REE concentrations normalized to chondritic concentrations (Sun and McDonough 1989) are shown for liquid compositions derived from average plagioclase, clinopyroxene, and orthopyroxene, and the range of normalized liquid concentrations derived from apatite are plotted against the ionic radius in angstroms of the REE (Shannon 1976)

interstitial liquid and (2) the buffering effect of the solid assemblage that will tend to keep the concentrations of compatible elements higher in the more evolved interstitial liquids than expected. As evolved interstitial liquids are returned to the main body of fractionating magma, they have significant potential to modify the magma's incompatible trace element fractionation trends (O'Hara and Fry 1996a, b). Saturation of accessory minerals, such as apatite, complicates the signature of these processes by depleting the returned liquid in elements that should be strongly enriched based on the bulk distribution coefficients in the fractionating silicate assemblage (Claeson and Meurer 2004). The crystallization of accessory minerals during compaction therefore has the potential to result in apparently disparate behavior of elements with similar incompatibilities in the fractionating assemblage (e.g., an enrichment in Zr relative to P and Nd). The buffering by the

Table 5 Mineral–liquid partition coefficients

Mineral	La	Ce	Pr	Nd	Sm	Eu	Gd	Tb	Dy	Y	Ho	Er	Tm	Yb	Lu
Apatite	6.8	6.4	5.9	5.6	5.2	5.2	4.9	4.8	4.6	–	4.3	4	3.7	3.5	3.4
Clinopyroxene	0.054	0.086	–	0.187	0.291	0.329	0.367	–	0.38	0.384	–	0.387	–	0.43	0.433
Plagioclase	0.049	0.040	–	0.025	0.015	0.235	0.0092	–	0.0045	0.0037	–	0.0029	–	0.0024	0.0022
Orthopyroxene	0.0024	0.0024	–	0.0055	0.0120	0.017	0.024	–	0.047	0.067	–	0.0831	–	0.147	0.191

Apatite Ds smoothed from estimates of Fleet and Pan (1997) that are based on the data of Chazot et al. (1996)
Clinopyroxene Ds are from the compilation of Bédard (2001)
Plagioclase and orthopyroxene Ds were calculated from mineral–mineral partition coefficients using the clinopyroxene Ds (see text)
Elements without values were not inverted to estimate liquid compositions in Fig. 10

solid assemblage should not significantly influence the differentiation of the main magma reservoir, but it will disguise the pathways that evolved liquids travel during their escape from the crystal pile. The buffering effect may also add confusion to identification of evolved interstitial liquids. For example, one might not expect high Sr and Ni contents in a liquid interstitial to a troctolite that has crystallized significant olivine and plagioclase (Meurer and Claeson 2002).

Depending upon the compositional path of the fractionating interstitial liquid and the extent of reaction with the cumulus assemblage, useful insights into parental liquid compositions may still be gained by modeling cumulates as though they formed in a closed system (i.e., with cumulus grains and an equilibrium liquid). This is because the interstitial liquid will follow essentially the same fractionation path throughout the compacting crystal pile (e.g., Meurer and Boudreau 1998a). As this interstitial liquid moves upward, a slightly more evolved liquid on the same fractionation path replaces it. If this process is uniform, then using the inversion approaches developed by Bédard (1994, 2001) to calculate liquid compositions involved in cumulate formation still proves useful. However, in systems where the interstitial liquid is reactive (e.g., Claeson and Meurer 2004) or when mechanical processes cause the loss of interstitial liquid to be less uniform, as in the development of porosity waves (Meurer and Boudreau 1996c), then these approaches must be modified. In either case, the estimates of the amount of "trapped liquid" have no physical significance.

As an example of why these estimates have no physical significance, we calculated the amount of "trapped liquid" for M105. We compare the observed bulk composition to the composition obtained by multiplying the weight percentage of each mineral by the average of the three most primitive mineral analyses of that mineral. The difference between the observed and calculated concentrations for each element provides an independent estimate of the amount of "trapped liquid" (Using the clinopyroxene partition coefficients to estimate an equilibrium "trapped liquid" composition). For M105 elements with bulk distribution coefficients less than 0.03, all yielded "trapped liquid" contents of less than 0.5%. The REE elements show a range in "trapped liquid" contents that is positively correlated with bulk distribution coefficients such that elements with distribution coefficients less than 0.1 (La, Ce, Nd) all predict less than ~2.5% "trapped liquid", those with coefficients between 0.1 and 0.125 (Sm, Gd, Dy, Er, Yb, Lu) predict between ~2.5 and 3.5% "trapped liquid", and Eu (which has a bulk distribution coefficient of 0.205) indicates that ~5% "trapped liquid" is present. The "trapped liquid" content of this sample varies by more than an order of magnitude depending upon the element used. Even within the REE there is too much variation to make the "trapped liquid" content of the rock a useful physical parameter.

Acknowledgements We thank D.T. Claeson for valuable discussions and editorial comments on early drafts of the manuscript. J.S. Scoates and A.E. Boudreau provided valuable criticisms in their role as reviewers and are thanked for their input. We thank T.L. Grove for his comments and editorial work in the preparation of this manuscript. This work was supported in part by NSF grant EAR-0229702.

References

Bédard JH (1994) A procedure for calculating the equilibrium distribution of trace-elements among the minerals of cumulate rocks, and the concentration of trace-elements in the coexisting liquids. Chem Geol 118:143–153

Bédard JH (2001) Parental magmas of the Nain Plutonic Suite anorthosites and mafic cumulates: a trace element modeling approach. Contrib Mineral Petrol 141:747–771

Boorman S, Boudreau AE, Kruger FJ (2004) The lower critical zone transition of the Bushveld Complex: a quantitative textural study. J Petrol 45:1209–1235

Boudreau AE, McCallum IS (1989) Investigations of the Stillwater Complex: part V. apatites as indicators of evolving fluid composition. Contrib Mineral Petrol 102:138–153

Cawthorn RG, Walsh KL (1988) The use of phosphorus contents in yielding estimates of the proportion of trapped liquid in cumulates of the Upper Zone of the Bushveld Complex. Mineral Mag 52:81–89

Chadam J, Hoff D, Ortoleva P, Sen A (1986) Reactive-infiltration instability. J Appl Math 36:207–238

Chazot G, Menzies MA, Harte B (1996) Determination of partition coefficients between apatite, clinopyroxene, amphibole, and melt in natural spinel lherzolites from Yemen: implications for wet melting of the lithospheric mantle. Geochem Cosmochim Acta 60:423–437

Cherniak DJ (2000) Rare earth element diffusion in apatite. Geochem Cosmochim Acta 64:3871–3885

Claeson DT, Meurer WP (2004) Fractional crystallization of hydrous basaltic "arc-type" magmas and the formation of amphibole-bearing cumulates. Contrib Mineral Petrol 147:288–304

Faul UH (1997) Permeability of partially molten upper mantle rocks from experiments and percolation theory. J Geophys Res 102:10299–10311

Fleet ME, Pan Y (1997) Rare earth elements in apatite: uptake from H_2O-bearing phosphate–fluoride melts and the role of volatile components. Geochem Cosmochim Acta 61:4745–4760

Fleet ME, Liu X, Pan Y (2000a) Rare-earth elements in chlorapatite [$Ca_{10}(PO_4)_6Cl_2$]: uptake, site preference, and degradation of monoclinic structure. Am Mineral 85:1437–1446

Fleet ME, Liu X, Pan Y (2000b) Site preference of rare earth elements in hydroxyapatite [Ca_{10} $(PO_4)_6(OH)_2$]. J. Solid State Chem 149:391–398

Haskin LA, Salpas PA (1992) Genesis of compositional characteristics of Stillwater AN-I and AN-II thick anorthosite units. Geochem Cosmochem Acta 56:1187–1212

Henderson P (1970) The significance of the mesostasis of basic layered igneous rocks. J Petrol 3:463–473

Kelemen PB, Whitehead JA, Aharonov E, Jordahl KA (1995) Experiments on flow focusing in soluble porous media, with application to melt extraction from the mantle. J Geophys Res 100:475–496

Langmuir CH (1989) Geochemical consequences of the solidification of magma chambers through "in situ" crystallization. Nature 340:199–205

Loferski PJ, Arculus R (1993) Multiphase inclusions in plagioclase from anorthosites in the Stillwater Complex, Montana: implications for the origin of the anorthosites. Contrib Mineral Petrol 114:63–78

Meurer WP, Boudreau AE (1996a) Petrology and mineral compositional features of the olivine-bearing zones of the Middle Banded series, Stillwater complex, Montana. J Petrol 37:583–607

Meurer WP, Boudreau AE (1996b) Evaluation of models of apatite compositional variability using apatite from the Middle Banded series of the Stillwater complex, Montana. Contrib Mineral Pet 125:225–236

Meurer WP, Boudreau AE (1996c) Compaction of density stratified cumulates: effect on trapped-liquid distributions. J Geol 104:115–120

Meurer WP, Boudreau AE (1998a) Compaction of igneous cumulates. Part I. Whole-rock compositions as an indicator of the trapped liquid proportions in the Stillwater complex, Montana. J Geol 106:281–292

Meurer WP, Boudreau AE (1998b) Compaction of igneous cumulates. Part II. Quantitative analysis of mineral laminations in the Stillwater complex, Montana. J Geol 106:293–304

Meurer WP, Claeson DT (2002) Evolution of crystallizing interstitial liquid in an arc-related cumulate determined by LA ICP-MS mapping of a large amphibole oikocryst. J Petrol 43:607–630

Meurer WP, Natland JH (2001) Apatite compositions from oceanic cumulates with implications for the evolution of mid-ocean ridge magmatic systems. J Volcan Geother Res 110:281–298

Meurer W, Klaber S, Boudreau AE (1997) Discordant bodies from olivine-bearing zones III and IV of the Stillwater Complex, Montana—evidence for postcumulus fluid migration and reaction in layered intrusions. Contrib Mineral Petrol 130:81–92

O'Hara MJ, Fry N (1996a) Geochemical effects of small packet crystallization in large magma chambers—further resolution of the highly compatible element paradox. J Petrol 37:891–925

O'Hara MJ, Fry N (1996b) The highly compatible trace element paradox—fractional crystallization revisited. J Petrol 37:859–890

Ross DK, Elthon D (1997) Cumulus and postcumulus crystallization in the oceanic crust; major and trace-element geochemistry of Leg 153 gabbroic rocks. In: Proceedings of ODP Sci results 153, pp 333–351

Shannon RD (1976) Revised effective ionic radii and systematic studies of interatomic distances in halides and chalcogenides. Acta Crystallog A32:751–767

Shirley DN (1986) Compaction of igneous cumulates. J Geol 94:795–809

Shirley DN (1987) Differentiation and compaction in the Palisades sill. J Petrol 28:835–865

Stormer JC, Pierson ML, Tacker RC (1993) Variation of F and Cl X-ray intensity due to anisotropic diffusion in apatite during electron microprobe analysis. Am Mineral 79:641–648

Sun S-s, McDonough WF (1989) Chemical and isotopic systematics of oceanic basalts; implications for mantle composition and processes. In: Saunders AD, Norry MJ (eds) Magmatism in the ocean basins. Geol Soc Special Pub 42:313–345

Wager LR, Brown GM (1967) Layered igneous rocks. W.H. Freeman Company, San Francisco, p 588

Willmore CC, Boudreau AE, Kruger FJ (2000) The halogen geochemistry of the Bushveld complex, Republic of South Africa: implications for chalcophile element distribution in the lower and critical zones. J Petrol 41:1517–1539